Materials Research. 2022; 25:e20220259
DOI: https://doi.org/10.1590/1980-5373-MR-2022-0259

Influence of the Number of Dimensions in the Impedance Spectroscopy Simulation of a YSZ Electrolyte

Ana Kaori de Oliveira Ouba*[a]*, Adilson Luiz Chinelatto[a], Janaina Semanech Borcezi[a], Ivo Neitzel[b], Adriana Scoton Antonio Chinelatto[a]

[a]Universidade Estadual de Ponta Grossa (UEPG), Programa de Pós Graduação em Ciência e Engenharia de Materiais (PPGECM), Departamento de Engenharia de Materiais, Carlos Cavalcanti Avenue, 4748, 84030-900, Ponta Grossa, PR, Brasil.
[b]Faculdade de Telêmaco Borba (FATEB), Mal. Floriano Peixoto, 1181, 84266-010, Telêmaco Borba, PR, Brasil.

Received: May 29, 2022; Revised: October 17, 2022; Accepted: October 25, 2022

The use of computer simulation to predict the behavior of devices and materials allows for the acceleration of system operation and reduces costs, as it eliminates the need to build prototypes for testing. This work proposes the construction of 3 models with different complexities to simulate the electrical behavior of a solid electrolyte fuel cell. Experimental data were compared with simulation data. The experimental data were obtained from the production of a solid YSZ by tape casting, sintered at 1550 °C. The material was characterized using impedance spectroscopy in atmospheric air. From the experimental data, a computer simulation was conducted by using commercial code (COMSOL Multiphysics v.5.4). The construction of the model was developed to 1D, 2D axisymmetric and 3D dimensions to simulate an electrolyte to use in cylindrical planar SOFC. Nyquist Impedance graphics were plotted for the three geometries in comparison with the experimental value. No variation was observed between the curves obtained by the different geometries for the same interface. In other words, the interface complexity did not interfere in the result obtained for the same experimental data. We concluded that the 1D model is ideal to predict the influence of operational parameters because it is simpler and saves analysis time, maintaining the reliability and accuracy of the results.

Keywords: *Impedance spectroscopy, solid oxide fuel cell, electrolyte, simulation model.*

1. Introduction

The electrolyte of a solid oxide fuel cell (SOFC) is a dense ion-conducting ceramic that transports ions between electrodes[1]. The most used materials in the manufacture of electrolytes for SOFCs are ceramics with a fluorite-like structure, mainly yttria-stabilized zirconia (YSZ)[2,3]. To fulfill their function, the electrolytes must have a relative density above 95% to prevent mixing of fuel and oxidizing gases, high ionic conductivity (above 0.1 $S.cm^{-1}$), low electronic conductivity (electronic transfer number less than 10^{-3}) and uniform thickness to reduce ohmic losses[4-7].

Electrochemical impedance spectroscopy (EIS), also known as alternating current (AC) impedance is among the most common methods of analysis performed for the electrical characterization of the electrolyte. This technique is based on the analysis of the response generated by the current when subjected to small sinusoidal disturbances in the electronic potential. Such disturbance is applied to a certain frequency range, which generally varies from 0.1 MHz to 30 MHz[8]. The variation in frequency makes it possible to differentiate the processes and mechanisms that occur on the surface of the electrodes and inside the electrolytes[9].

The main difficulty in the study and development of SOFCs is the operating temperature of the electrolyte, which works around 1000 K, limiting the choice of materials, and reducing the life of the device due to thermal degradation and corrosion of the materials. This also makes it difficult and expensive to build new systems[10]. Due to these challenges, the interest in solving problems through computer simulation has increased. This resource allows the acceleration of the system operation in time, makes it possible to predict possible accidents that could occur during the implementation of a real system and saves economic resources, as it eliminates the need to build prototypes for testing[11]. However, the construction and complexity of the model to be used in the simulations is one of the biggest challenges to use these simulations extensively in the search for new materials.

Simulation is a computational tool used to study physical and chemical phenomena that, together with modeling, makes it possible to describe a system through a set of known equations and laws[12].

The modeling of the SOFC cell can be studied as a function of the transport phenomena in fluids using Computational Fluid Dynamics (CFD) by applying the Finite Element Method (FEM). Fluids are ruled by differential equations that represent mass and energy conservation laws. Depending

*e-mail: anaouba@hotmail.com

on the phenomena to be studied, or, the formulation of the problem, there are three study depths determined by their dimensions (Table 1 and Figure 1).

There is also the 2D axisymmetric model which consists of a three-dimensional model expressed in cylindrical coordinates (r,θ,z) that undergoes an integration of the variable θ and becomes a two-dimensional problem (r,z)[13].

The simpler the domain is, the easier it will be to understand the influence of different reactions on an electrochemical system, in addition to facilitating the convergence of the problem and providing a good estimate of the current voltage behavior[14]. In this way, a 2D axisymmetric model represents a simplification of a three-dimensional domain, where only the revolution section needs to be discretized (Figure 2).

The characterization of the electrical behavior of SOFC components can be carried out by electrochemical impedance spectroscopy (EIS). This technique consists of evaluating the response of the material to the application of an alternating voltage and measuring the real and imaginary parts of the complex impedance as a function of frequency. The real part corresponds to the resistive part and the imaginary part corresponds to the part of capacitive and inductive reactance[15]. The response of the material to the application of this signal provides semicircles that represent the contributions of electrical properties associated with electrodes and contacts, grain boundaries and bulk of the grains[16,17]. Each semicircle can be associated with the behavior of resistive, capacitive and inductive elements combined in equivalent circuits formed by resistors (R), capacitors (C) and inductors (L). In practice, most samples do not exhibit an ideal behavior, that is, generally the arcs appear flat, revealing a high angle of decentralization and suggesting the presence of phenomena with different time constants[18]. In such cases, the non-Debye relaxation phenomenon occurs, which results in Constant Phase Element (CPE) in equivalent electrical circuits. This is due to the heterogeneities between the characteristics of each grain, as well as the heterogeneities between the characteristics of each grain boundary combined in series/parallel connections[19].

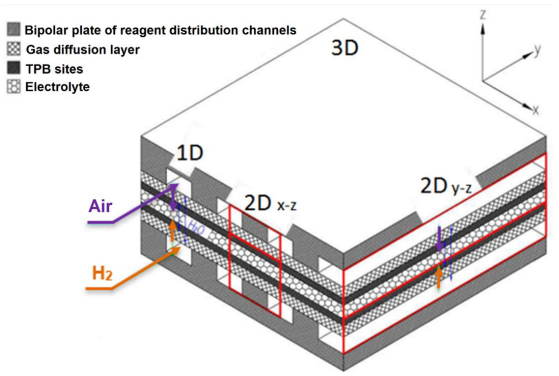

Figure 1. Modeling domains applicable in the characterization of the problem to be analyzed.

Before starting the construction of a model, in addition to choosing the dimension of the study domain, it is necessary to evaluate and define the best interface to analyze the problem. Regarding the EIS evaluation, there are three possibilities of current distribution interfaces: primary, secondary and tertiary[20].

The secondary current distribution interface considers activation overpotentials, but disregards possible changes in electrolyte composition. It defines the transport of charged ions in a uniform electrolyte. The current conduction in the electrodes and electrolytes is calculated using Ohm's law in combination with a charge balance. The relationship between charge transfer and activation overpotentials is made by arbitrary kinetic expressions such as the Butler-Volmer and Tafel equations. Neumann boundary conditions are used to describe current flow conditions. This interface can also be combined with mass transport interfaces to describe concentration-dependent current distributions.

This work aimed to develop and validate an EIS model for SOFC from experimental data of an YSZ electrolyte with platinum electrodes. The model construction was developed for 1D, 2D axisymmetric and 3D dimensions to simulate an electrolyte to be used in cylindrical planar SOFC. The three dimensions were evaluated via the secondary current distribution interface available in the commercial code (COMSOL Multiphysics v.5.4).

Table 1. Modeling domains applicable in the characterization of problems according to the design.

Dimension	Axis	Region	Analysis
1D	z	Electrolyte TPB sites	Reagent flow Reagent concentration Temperatures Electrical and electrochemical potentials
2D	y-z x-z	Electrolyte TPB sites Gas diffusion region Canals	Reagent flow Reagent concentration and products Temperatures Electric and ionic potentials
3D	x-y-z	Electrolyte TPB sites Gas diffusion region Canals	Reagent flow Charge losses Reagent concentration and products Temperatures Heat removal Electric and ionic potentials

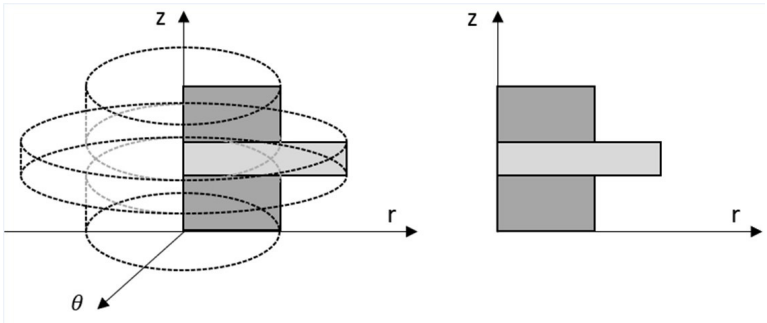

Figure 2. Domain and contour simplification in axisymmetric cases.

2. Experimental

2.1. YSZ fabrication and characterization

The YSZ electrolyte, formed from the tape casting process, was sintered at a 2°C/min heating rate up to 600°C to avoid warping of the sample during the removal of the organic components and then it was heated at a 10°C/min rate up to 1550°C with a 4-hour threshold for sintering and component densification. After sintering, the sample was characterized by evaluating the apparent density (AD), apparent porosity (AP), X-ray diffraction (XRD) and electrochemical impedance spectroscopy (EIS).

For the AD and AP calculations, the dry mass of the sample (m_{dry}) was measured after remaining 24 hours at 110°C in an oven. Then, measurements of the mass of the immersed sample ($m_{immersion}$) were carried out in the hydrostatic balance after remaining immersed in distilled water for 24 hours and, finally, measurements of the mass of the wet sample (m_{wet}) were carried out, which consists of the measurement in the air of the same sample previously immersed[18].

The mass values were applied to Equation 1 to determine AD (g/cm^3) and in Equation 2 to determine PA (%)[18]:

$$AD = \frac{m_{dry}}{m_{wet} - m_{immersion}} \times \rho_{H_2O} \quad (1)$$

$$AP = \frac{m_{wet} - m_{dry}}{m_{wet} - m_{immersion}} \times 100 \quad (2)$$

The XRD data were obtained using a Shimadzu diffractometer with Kα(Cu) radiation = 1.54060 Å, in an angular variation range of 2θ from 5° to 90°, and a 2°/minute scan speed. Phase identification was performed using the software Crystallographica Search-Match.

Platinum electrodes were deposited (Fuel Cell Materials) to evaluate the YSZ sample electrical properties. The EIS measurement was performed in atmospheric air with a disturbance amplitude signal of 300 mV, measuring the real and imaginary parts of the complex impedance as a function of frequency between 1 Hz and 1 MHz[8]. The analysis results were interpreted using the software Frequency Response Analyzer (FRA), which obtains the results directly from the potentiostat and transmits them to the software Zview® Version 3.0. used to evaluate the results obtained. This software employed equivalent circuits to determine the resistance of the material, which was converted into resistivity through Equation 3:

$$\rho = \frac{R.A}{e} \quad (3)$$

Where:
ρ: resistivity (Ω.m)
R: electrical resistance (Ω)
A: sample section area (m^2)
e: sample thickness (m)
Resistivity is the inverse of conductivity, as Equation 4:

$$\rho = \frac{1}{\sigma} \quad (4)$$

2.2. Simplifications of the computational model

The commercial code (COMSOL Multiphysics v.5.4) was used to obtain the mathematical model. This software has a pre-installed fuel cell module with tools to model electrochemical reactions and transport phenomena[21].

Some concepts are currently accepted for the construction of a simplified mathematical model study[22]:

a) All reactants and products are in the gas phase, in other words, there is no phase change in any of the cell regions;
b) The gases were considered ideal;
c) The flow is incompressible and laminar due to the fact that the pressure gradients and the flow velocity are small;
d) The electrolyte is impermeable to gases, in other words, the losses by permeation of reagents are disregarded;
e) The structure and composition of SOFC components are considered isotropic and homogeneous;
f) The cell operates under isothermal conditions;
g) The ohmic losses are disregarded in solid components;
h) The SOFC operates in a stationary state.

The model construction was developed for the dimensions 1D, 2D axisymmetric and 3D to simulate a cylindrical planar SOFC. The three dimensions were evaluated by the secondary current distribution interface.

2.3. Geometries

During the fabrication of the SOFC, the component used as a support must be thick to provide mechanical stability

to the unit cell. In electrolyte-supported cells, the YSZ membrane usually has a typical thickness of 1.5 x 10^{-4} m[23].

Figure 3 illustrates planar cylindrical geometry in 1D space. The lengths shown in the figure indicate the thickness of the components. Thus, we established that the thickness of the electrolyte was equal to 1.5 x 10^{-4} m and that the thickness of the electrodes was equal to 1.0 x 10^{-4} m. The isolation was applied to the extremities of the electrodes.

As described earlier, the 2D axisymmetric geometry represents the SOFC revolution section Figure 4 illustrates the planar cylindrical geometry in the 2D axisymmetric space. In this geometry, the thickness of the components corresponds to the length used in the 1D formulation. We established that the electrolyte diameter, which is the supporting component, was equal to 1.2 x 10^{-2} m. The diameter of the electrodes was 7.2 x 10^{-3} m.

The 3D geometry best represents a real model. Figure 5 illustrates the planar cylindrical geometry in the 3D space. The dimensions of the three-dimensional model are the same as those used for the previous models.

The three geometries were built in COMSOL Multiphysics® using the geometry node. Table 2 shows a detail of the parameters used for the construction of the three studied geometries.

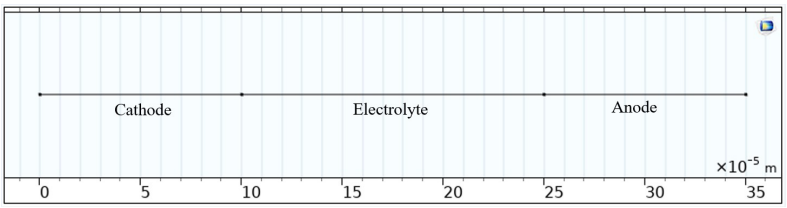

Figure 3. Planar cylindrical geometry in 1D space.

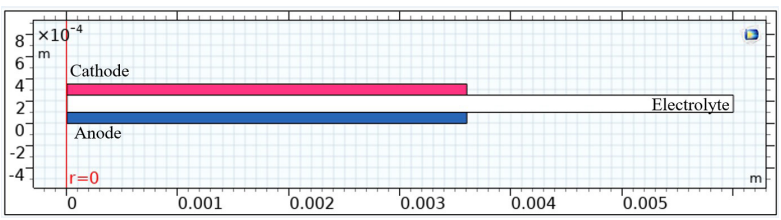

Figure 4. Planar cylindrical geometry in 2D axisymmetric space.

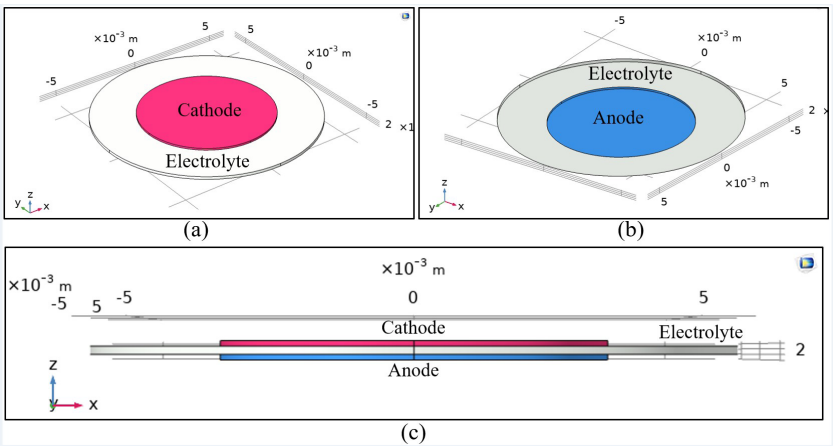

Figure 5. Planar cylindrical geometry in 3D space: a) higher perspective view; b) bottom perspective view; c) side view.

Table 2. Geometric parameters used to build 1D, 2D and 3D models.

Description of geometric parameters	1D model	2D model	3D model
Electrolyte thickness	1.5 x 10^{-4} m	1.5 x 10^{-4} m	1.5 x 10^{-4} m
Thickness of platinum electrodes	1.0 x 10^{-4} m	1.0 x 10^{-4} m	1.0 x 10^{-4} m
Electrolyte radius	-	6.0 x 10^{-3} m	6.0 x 10^{-3} m
Radius of platinum electrodes	-	3.6 x 10^{-3} m	3.6 x 10^{-3} m
Electrolyte diameter	-	-	1.2 x 10^{-2} m
Diameter of platinum electrodes	-	-	7.2 x 10^{-3} m

2.4. Secondary current distribution interface nodes and equations

2.4.1. Electrolyte and porous electrode node

The secondary current distribution interface is constructed and deduced from the mass conservation equation, which can be described by the equations for each species i diluted in an electrolyte, according to Equation 5[24]:

$$\frac{\partial c_i}{\partial t} + \nabla \bullet N_i = R_{i,tot} \tag{5}$$

Where:
N_i is the total flow of species i (mol/(m^2·s)).
$R_{i,tot}$ is the total reaction rate for species i (mol/(m^3·s)).

From the simplification of the study in stationary state, the variation of the concentration as a function of time is eliminated from Equation 5, remaining only the N_i gradient.

The N_i magnitude is obtained by the Nernst-Planck equations, which present the species flux as a set of transport mechanisms by diffusion, migration and convection, shown in the respective order on the right side of Equation 6:

$$N_i = -D_i \nabla c_i - z_i u_{m,i} F c_i \nabla \phi_l + c_i u \tag{6}$$

Where:
c_i is the concentration of ion i (mol/cm^3)
z_i is the valence of ion i
D_i is the diffusion coefficient (cm^2/s)
$u_{m,i}$ is mobility (s · mol / kg)
F is Faraday's constant (96485 C/mol)
$\nabla \phi_l$ is the electrolytic potential gradient (V)
u is the ion velocity vector (cm/s) for reaction m (oxidation or reduction)

The current density in the electrolyte (i_l) in A/m^2 can be described using the sum of all fluxes of species i, according to Equation 7:

$$i_l = F \sum z_i N_i \tag{7}$$

Assuming an electroneutrality condition and neglecting the charge-carrying ion concentration gradients, the current density is simplified by Equation 8:

$$i_l = -F^2 \sum z_i^2 u_{m,i} c_i \phi_l \tag{8}$$

Assuming that the composition of charge carriers is constant, the electrolytic conductivity $\sigma_l \ (\Omega.cm)^{-1}$ can be defined by Equation 9:

$$\sigma_l = F^2 \sum z_i^2 u_{m,i} c_i \tag{9}$$

In this way, the current density in the electrolyte will be equivalent to the product between the conductivity and the ionic potential gradient, in other words, it has the same form as Ohm's law, as shown in Equation 10[25]:

$$i_l = -\sigma_l \nabla \Phi_l \tag{10}$$

As Ohm's law is also used to conduct current in the solid electrode phase, Equation 11 will give the general equation for the electrodes:

$$i_s = -\sigma_s \nabla \Phi_s \tag{11}$$

Where:
i_s is the current density in the solid electrode (A/cm^2)
σ_S is the conductivity of the solid electrode $(\Omega.cm)^{-1}$
$\nabla \phi_S$ is the potential gradient of the solid electrode (V)

Ohm's law is used in combination with a charge balance to describe the current flow through the electrodes. In this way, the secondary current distribution interface defines two dependent variables, one for the electrolyte potential (Φ_s). These variables are the current source densities (Q), which vary as a function of the current density gradient ($\nabla \bullet i$), as shown in Equation 12:

$$\nabla \bullet i_s = Q_s \tag{12}$$

Where:
Q_s is the source of electron current in the electrode (A/cm^3)
$\nabla \bullet i_s$ is the current density gradient of the electrode

Similarly, Equation 13 gives the electrolyte current source:

$$\nabla \bullet i_l = Q_l \tag{13}$$

Where:
Q_l is the ion current source in the electrolyte (A/cm^3)
$\nabla \bullet i_l$ is the electrolyte current density gradient

The advantage of the ohmic expression is the linear relationship of current density to ionic potential for secondary current distribution.

2.4.2. Sub-node reaction in the porous electrode

The secondary current distribution interface considers the activation overpotential (η), which is specific for a reaction taking place at the interface and depends on the electron potential at the electrode (Φ_s) and the ionic potential (Φ_l), according to Equation 14[26]:

$$\eta_m = \Phi_s - \Phi_l - E_{eq,\,m} \tag{14}$$

Where:
$E_{eq,\,m}$ is the reaction m equilibrium potential.

The corresponding potential difference in Φ_l, called ohmic drop, alters the electrochemical equilibrium position. In this case, an additional potential in the electrical circuit may be required to generate an equivalent overpotential.

The electrode kinetics settings will define the local current density i_{loc} (A/cm^2) at the interface between electrolyte and electrode. This value will depend on the overpotential (η) and the equilibrium potential ($E_{eq,\,m}$). For all expressions, the exchange current density i_0 (A/cm^2) is a measure of kinetic activity.

The Butler-Volmer equation describes the current density due to an electrochemical reaction as a function of overpotential and reactant and product concentrations for a reversible process. If the kinetics do not depend on the concentration, the general form of the Butler-Volmer equation is given by Equation 15[26]:

$$i_{loc,m} = i_0 \left(\exp\left(\frac{\alpha_a F \eta}{RT} \right) - \exp\left(\frac{-\alpha_c F \eta}{RT} \right) \right) \tag{15}$$

Where:
$i_{loc,m}$ is the local charge transfer current density for reaction m

The equation above describes the electrode kinetics and it is used in the "porous electrode reaction" node. The parameters of the anodic charge transfer coefficient α_a (dimensionless) and cathodic charge transfer α_c (dimensionless) will affect how much the i_{loc} will change with changes in overpotential.

2.4.3. Electrical double layer capacitance sub-node

As described earlier, the Butler-Volmer expression is used to calculate the magnitude of the electrolysis current or faradaic current. Nonetheless, the interface between the electrodes and the electrolyte can consume capacitive current due to the attraction or repulsion of ions, creating a layer of oppositely charged ions close to the electrode.

The charge layer on the electrode and the opposite charge layer on the adjacent electrolyte are called double layer and can be thought of as a parallel plate capacitor. The charge will vary with the current density at the electrode.

The physics of the structure and formation of two layers is highly complex and not yet well understood. One of the simplest empirical methods to explain the observed influence of capacitance on polarization curves is to introduce a constant ideal capacitance at the interface between the electrode and the electrolyte.

In the double layer region of SOFCs with YSZ electrolyte, the current density is zero and the capacitance presents values of tenths of $\mu F / cm^2$ for temperatures higher than 700°C[27].

2.4.4. Harmonic perturbation

The EIS technique, also known as alternating current (AC) impedance, is based on the analysis of the response generated by the current when subjected to small sinusoidal perturbations in the electronic potential. This perturbation is applied to a certain range of frequencies, which makes it possible to differentiate the processes and mechanisms that occur on the surface of the electrodes[28].

The harmonic disturbance node is used to specify the amplitude of the voltage or current disturbance applied in the frequency domain, which can vary according to the study or boundary condition selected.

2.4.5. Boundary conditions

The boundary conditions of the secondary current distribution interface are given by the nodes pre-installed in the study interface, which are the isolation of the walls, the initial values of the dependent variables, the electrolyte potential at the electrode boundary and the current of the electrode bordering the electrolyte[14].

The isolation boundary condition describes that the walls of a cell or cell boundaries are in contact with a conductor. The boundary condition is shown in Equation 16[14]:

$$i_k \cdot \mathbf{n} = 0 \tag{16}$$

Where:
i_k is the current density vector for electrolyte (l) or electrode (s)
n is the normal flow vector of the molar species.

The second boundary condition is related to the initial values of the dependent variables, that is, de Φ_s e Φ_l, according to Equation 17 and Equation 18:

$$\Phi_s = 0 \tag{17}$$

$$\Phi_l = 0 \tag{18}$$

Finally, an electrolyte potential node is added to organize the boundary conditions at the boundary between the electrode and the electrolyte. These conditions are related to the electrolyte potential (Φ_l) in this region according to Equation 19:

$$\Phi_l = \Phi_{l,bnd} = 0 \tag{19}$$

Moreover, with the electrode current in the boundary region according to Equation 20:

$$\int_{\partial\Omega} i_s \cdot \mathbf{n}\, dp = i_{s,\,average} \int_{\partial\Omega} dp \tag{20}$$

Where:
$\partial\Omega$: is the boundary area between the electrolyte and the electrode
$\Phi_{l,bnd}$: is the electrolyte potential at the boundary between the electrolyte and the electrode
$i_{s,\,average}$: is the average current density at the electrode.

The value of current density at the electrode (i_s) is considered constant and it has a magnitude equal to $i_{s,average}$. The use of the value of $i_{s,average}$ aims to mitigate an unequal potential distribution at the boundary between the electrolyte and the electrode.

2.5. Summary of equations and parameters used

The nodes and sub-nodes added to the secondary current distribution interface are summarized in Table 3.

The parameters used in the simulation interface are shown in Table 4.

3. Results and Discussion

3.1. YSZ characterization

Figure 6 shows the YSZ sample XRD results after sintering and removing the organic compounds at 1550°C.

The analysis shows that the only phase detected was cubic Yttria Stabilized Zirconia ($Y_{0,15}Zr_{0,85}O_{1,93}$), according to datasheet 30-1468 from the software *Crystallographica Search-Match*, no trace of other impurities was observed. Datasheet comments describe the composition as being a common composition to use in solid state electrolytes.

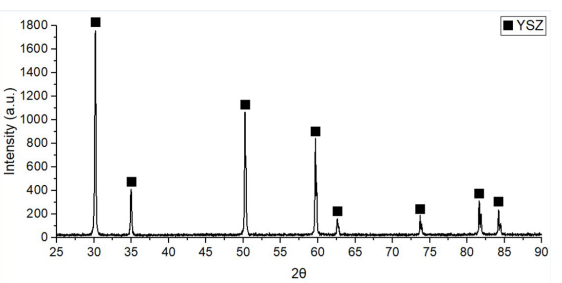

Figure 6. XRD of YSZ.

Table 3. Nodes, sub-nodes and equations used in the simulation interface.

Node or sub-node	Equation used	Formula	Ref
Electrolyte	Ohm's Law with charge balance	$\nabla \bullet i_l = Q_l$ $i_l = -\sigma_l \nabla \Phi_l$	Daneshvar et al.[25]
Isolation	Boundary condition	$i_k \bullet n = 0$	COMSOL[14]
Initial values	Boundary condition	$\Phi_s = 0$ $\Phi_l = 0$	COMSOL[14]
Porous electrode	Ohm's Law with charge balance	$\nabla \bullet i_s = Q_s$ $i_s = -\sigma_s \nabla \Phi_s$	Singhal and Kendal[26]
Reaction at the porous electrode	Butler-Volmer Kinetics	$i_{loc,m} = i_0 \left(\exp\left(\frac{\alpha_a F \eta}{RT} \right) - \exp\left(\frac{-\alpha_c F \eta}{RT} \right) \right)$	Singhal and Kendal[26]
Electrical double layer capacitance	Boundary condition	$i_{dl} = 0$ $C_{dl} \neq 0$	COMSOL[14]
Electrolyte potential	Boundary condition	$\Phi_l = \Phi_{l,bnd} = 0$	COMSOL[14]
Current in the electrode	Boundary condition	$\int_{\partial\Omega} i_s \bullet n \, dp = i_{s,\ average} \int_{\partial\Omega} dp$	COMSOL[14]
Harmonic perturbation	–	It depends on selected boundary condition	Experimental

Table 4. Parameters used in the secondary distribution interface.

Parameter	Symbol	Value	Ref
Platinum conductivity	k	3.9 x 10^4 S/cm	Burkov et al.[29]
YSZ conductivity	σ	1.8 x 10^{-4} S/cm	Experimental
Temperature	T	973 K	Experimental
Equilibrium potential	E_{eq}	0.95 V	Choi et al.[30]
Anodic transfer coefficient	α_a	3.5	Dickinson[31]
Cathodic transfer coefficient	α_c	0.5	Andersson et al.[32]
Average current density of the electrode	i_{avg}	-0,05 x 10^{-6} A/cm^2	Experimental
Perturbation amplitude	Δi_{avg}	0.9 A/cm^2	Experimental
Exchange current density	i_0	4 x 10^{-3} A/m^2	Okamoto et al.[33]
Double layer capacitance	C_{dl}	0.01 F/m^2	Ge et al.[27]

Table 5. Resistance and conductivity obtained by EIS.

	YSZ – Atmospheric air							
$T\ (°C)$	350	400	450	500	550	600	650	700
$R\ (\Omega)$	1695.0	483.3	145.2	52.1	23.1	12.5	7.9	5.2
$\sigma\ (S/cm)$	$5.8\ x\ 10^{-5}$	$2.0\ x\ 10^{-4}$	$6.8\ x\ 10^{-4}$	$1.9\ x\ 10^{-3}$	$4.3\ x\ 10^{-3}$	$7.9\ x\ 10^{-3}$	$1.3\ x\ 10^{-2}$	$1.8\ x\ 10^{-2}$

The composition reference consists of ZrO_2 doped with 8% by mol of Y_2O_3 sintered at 1400 °C for six days[34].

As previously described, the materials used as electrolytes need to have low porosity (below 5%). The average apparent porosity measured in four specimens, as described in item 3.1, was 3.44% and the average apparent density was 5.63 g/cm^3. The theoretical density of YSZ is 5.9 g/cm^3 [35], since the apparent density obtained was 95.4% of the theoretical density (TD), it is possible to affirm that the material presents the necessary values for application as an electrolyte in SOFC and that the parameters and procedures used for sintering were effective to promote the minimum densification necessary.

Finally, the analysis of the impedance spectra by the ZView software allowed us to obtain the resistance values to calculate the electrical conductivity of the YSZ electrolyte at temperatures between 350 and 700 °C.

Table 5 shows comparisons with the electrical resistance value and total conductivity of the components at temperatures

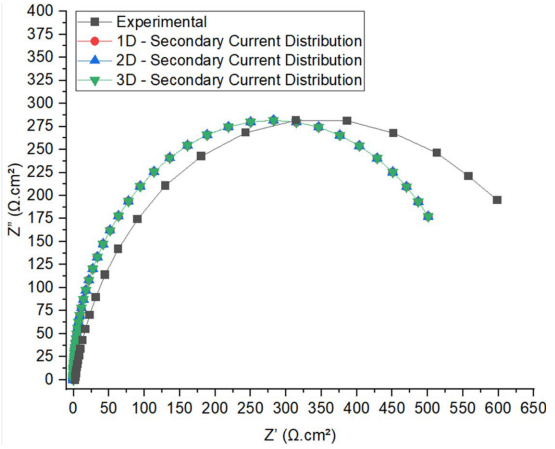

Figure 7. Nyquist Impedance vs. Ground (Ω.cm^2) for secondary current distribution interface compared to experimental value.

between 350 and 700 °C. The area of the deposited electrode is equal to 0.38 cm^2.

The conductivity values for the YSZ were similar to those values found in the literature, that is, they must be greater than 10^{-3} S/cm for temperatures above 600 °C[36] and greater than 10^{-2} S/cm to be able to be used as electrolytes in SOFC[37,38]. Due to this fact, the computer simulation was performed at 700 °C, as it presented the highest values of total conductivity.

3.2. Secondary current distribution interface

For the secondary current distribution interface, an intensity of 4 x 10^{-7} A/cm^2 was used for the exchange current density and a value of 1 x 10^{-6} F/cm^2 for the double layer capacitance. Figure 7 shows the Nyquist plots of Impedance vs. Ground (Ω.cm^2) for the three studied geometries in comparison with the experimental value.

The equivalent circuit used to fit the plots is presented in Figure 7 and is composed of a resistor (R1) connected in series to another resistor (R2) connected in parallel to a constant phase element (CPE1). The value of R1 corresponds to the charge transfer resistance equivalent to the polarization resistance of the sample.

Comparatively, the experimental curve presented very close values for the imaginary part, which corresponds to the capacitive terms. However, it presented a difference in the real part, which corresponds to the resistive terms. That difference in the resistive terms indicates that the real resistance is greater than the resistance calculated by the simulation, probably due the simplifications applied in sub-item 3.2 that disregard the material defects and changes in flow gases during the measurements. Nonetheless, this difference was already expected and did not affect the result obtained, since the computer simulation is performed in order to estimate the behavior of a given material.

It was possible to observe that there was no variation between the plots obtained by the different geometries for the same interface. In other words, the complexity of the interface did not interfere in the result obtained for the same experimental data. However, the greater the number of dimensions studied is, the greater the number of degrees of freedom is and, consequently, the longer the time needed to solve the simulation is.

Table 6. Number of freedom degrees and solution time for the different geometries used in each interface studied.

Geometry	Number of freedom degrees	Solution Time
1D	44	25 s
2D	938	41 s
3D	76886	499 s

Table 6 shows the values of freedom degrees and solution time for the geometries studied at the two interfaces.

The number of freedom degrees quantifies the credibility of each uncertainty component. In general, the freedom degree is the total number of measurements (N) minus one, so it can be said that a high degree of credibility implies a high freedom degree[39].

The study carried out for 3D geometries presents a high degree of credibility according to the respective numbers of freedom degrees. Nonetheless, this implies a longer solution time and a greater difficulty in the convergence of the problem. The use of the 1D model simplifies the problem and saves time in observing the influence of operational parameters, maintaining the reliability and accuracy of the results.

4. Conclusions

Comparatively, the simulation data were very similar to the experimental value for the exchange current density and double layer capacitance values used. The assumptions made at the time of construction of the mathematical model to simplify and adapt it to the study carried out were consistent with the experimental results.

The secondary current distribution interface and the literature values stipulated (Table 4) allowed a good approximation of the simulation and experimental results. Finally, the model built for the three studied geometries showed no variation between the curves obtained, that is, the complexity of the interface did not interfere with the result obtained for the same experimental data. Thus, we concluded that the use of the 1D model is ideal, as it simplifies the problem and saves time in observing the influence of operational parameters, maintaining the reliability and accuracy of the results.

5. Acknowledgments

The authors gratefully acknowledge the financial support from the Brazilian research funding agency CAPES - Brazil (National Council for the Improvement of Higher Education) and CNPq - Brazil (National Council for Scientific and Technological Development).

6. References

1. Hoogers G. Fuel cell technology handbook. 1st ed. Boca Raton: CRC Press; 2002.
2. Biswas M. Electrolyte materials for solid oxide fuel cell. J Powder Metallurgy & Mining. 2013;2(3):e114.
3. Sawant P, Varma S, Wani BN, Bharadwaj SR. Synthesis, stability and conductivity of $BaCe_{0.8-x}Zr_xY_{0.2}O_{3-\delta}$ as electrolyte for proton conducting SOFC. Int J Hydrogen Energy. 2012;37(4):3848-56.

4. Kim Y, Jo H, Allen JL, Choe H, Wolfenstine J, Sakamoto J. The effect of relative density on the mechanical properties of hot-pressed cubic $Li_7La_3Zr_2O_{12}$. J Am Ceram Soc. 2016;99(4):1367-74.
5. Mahato N, Gupta A, Balani K. Doped zirconia and ceria-based electrolytes for solid oxide fuel cells: a review. Nanomater Energy. 2012;1(1):27-45.
6. Dusastre V, Kilner JA. Optimisation of composite cathodes for intermediate temperature. Solid State Ion. 1999;126(1-2):163-74.
7. Koehler TM, Jarrell DB, Bond LJ. High temperature ceramic fuel cell measurement and diagnostics for application to solid oxide fuel cell systems. USA: Pacific Northwest National Laborator; 2001.
8. Huang QA, Hui R, Wang B, Zhang J. A review of AC impedance modeling and validation in SOFC diagnosis. Electrochim Acta. 2007;52(28):8144-64.
9. Jamalabadi MYA. Simulation of electrochemical impedance spectroscopy of a solid oxide fuel cell anodes. World Appl Sci J. 2014;32(4):667-71.
10. Smithsonian Institution. Fuel cells solid oxide fuel cells [Internet]. Washington: National Museum of American History; 2020 [cited 2022 May 29]. Available from: http://americanhistory.si.edu/fuelcells/so/sofcmain.htm
11. Sánchez PJ. Fundamentals of simulation modeling. In: IEEE 2007 Winter Simulation Conference; 2007; Washington. Proceedings. New York: IEEE; 2007. p. 54-62.
12. Sharifi SM, Rowshanzamir S, Eikani MH. Modelling and simulation of the steady-state and dynamic behaviour of a PEM fuel cell. Energy. 2010;35(4):1633-46.
13. Delouei AA, Emamian A, Karimnejad S, Sajjadi H. A closed-form solution for axisymmetric conduction in a finite functionally graded cylinder. Int Commun Heat Mass Transf. 2019;108:104280.
14. COMSOL Application Gallery. Current density distribution in a solid oxide fuel cell [Internet]. Grenoble: COMSOL Multiphysics; 2022 [cited 2022 May 29]. Available from: https://br.comsol.com/model/current-density-distribution-in-a-solid-oxide-fuel-cell-514
15. Rodrigues S, Munichandraiah N, Shukla AK. A review of state-of-charge indication of batteries by means of a.c. impedance measurements. J Power Sources. 2000;87(1-2):12-20.
16. Hofmann P, Panopoulos KD. Detailed dynamic solid oxide fuel cell modeling for electrochemical impedance spectra simulation. J Power Sources. 2010;195(16):5320-39.
17. Masteghin MG, Orlandi MO. Grain-boundary resistance and nonlinear coefficient correlation for SnO_2-based varistors. Mater Res. 2016;19(6):1286-91.
18. Shukla A, Choudhary RNP, Thakur AK. Effect of Mn^{4+} substitution on thermal, structural, dielectric and impedance properties of lead titanate. J Mater Sci Mater Electron. 2009;20(8):745-55.
19. Jorcin J-B, Orazem ME, Pébère N, Tribollet B. CPE analysis by local electrochemical impedance spectroscopy. Electrochim Acta. 2006;51(8-9):1473-9.
20. Pfaffe M. Current density distribution interface use [Internet]. Grenoble: COMSOL Multiphysics; 2014 [cited 2022 May 29]. Available from: https://www.comsol.com/blogs/current-distribution-interface-use
21. COMSOL Product Suite. Fuel cell & electrolyzer module [Internet]. Grenoble: COMSOL Multiphysics; 2022 [cited 2022 May 29]. Available from: https://www.comsol.com/fuel-cell-and-electrolyzer-module
22. Fox RW, Pritchard PJ, McDonald AT. Introduction to fluids mechanics. 8th ed. USA: John Wiley & Sons; 2011.
23. Virkar AV, Chen J, Tanner CW, Kim J-W. The role of electrode microstructure on activation and concentration polarizations in solid oxide fuel cells. Solid State Ion. 2000;131(1-2):189-98.
24. Wu S-L, Orazem ME, Tribollet B, Vivier V. The influence of coupled faradaic and charging currents on impedance spectroscopy. Electrochim Acta. 2014;131:3-12.
25. Daneshvar K, Fantino A, Cristiani C, Dotelli G, Pelosato R, Santarelli M. Multi-physics simulation of a circular-planar anode-supported solid oxide fuel cell. In: COMSOL Conference; 2012; Milan. Proceedings. Grenoble: COMSOL; 2012.
26. Singhal SC, Kendal K. High temperature and solid oxide fuel cells: fundamentals, design and applications. 1st ed. USA: Elsevier Science; 2003.
27. Ge X, Fu C, Chan SH. Double layer capacitance of anode/solid-electrolyte interfaces. Phys Chem Chem Phys. 2011;13(33):15134-42.
28. Bessler WG. A new computational approach for SOFC impedance from detailed electrochemical reaction-diffusion models. Solid State Ion. 2005;176(11-12):997-1011.
29. Burkov AT, Heinrich A, Konstantinov PP, Nakama T, Yagasaki K. Experimental set-up for thermopower and resistivity measurements at 100-1300 K. Meas Sci Technol. 2001;12(3):264-72.
30. Choi D-W, Ohashi M, Lozano CA, Vanzee JW, Aungkavattana P, Shimpalee S. Sulfur diffusion of hydrogen sulfide contaminants to cathode in a micro-tubular solid oxide fuel cell. Electrochim Acta. 2019;321(20):134713.
31. Dickinson E. Electrochemical impedance spectroscopy: experiment, model, and app [Internet]. Grenoble: COMSOL Multiphysics; 2017 [cited 2022 May 29]. Available from: https://br.comsol.com/blogs/electrochemical-impedance-spectroscopy-experiment-model-and-app/
32. Andersson M, Paradis H, Yuan J, Sundén B. Three dimensional modeling of an solid oxide fuel cell coupling charge transfer phenomena with transport processes and heat generation. Electrochim Acta. 2013;109(30):881-93.
33. Okamoto H, Kawamura G, Kudo T. Study of oxygen adsorption on platinum through observation of exchange current in a solid electrolyte concentration cell. Electrochim Acta. 1983;28(3):379-82.
34. Ptoertsch M. ICDD grant-in-aind. Pennsylvanis: Penn State University, University Park.
35. Panthi D, Hedayat N, Du Y. Densification behavior of yttria-stabilized zirconia powders for solid oxide fuel cell electrolytes. J Adv Ceram. 2018;7(4):325-35.
36. Han MF, Yang ZB, Liu Z, Le HR. Fabrication and characterizations of YSZ electrolyte films for SOFC. Key Eng Mater. 2010;434-435:705-9.
37. Steele BCH, Heinzel A. Materials for fuel-cell technologies. Nature. 2001;414(6861):345-52.
38. Menzler NH, Tietz F, Uhlenbruck S, Buchkremer HP, Stover D. Materials and manufacturing technologies for solid oxide fuel cells. J Mater Sci. 2010;45(12):3109-35.
39. Ellison SLR, Rosslein M, William A. Guide CG 4: quantifying uncertainty in analytical measurement. 2nd ed. USA: Eurachem/Citac; 2000.